Electronic Structural Contributions to *g* Values and Molybdenum Hyperfine Coupling Constants in Oxyhalide Anions of Molybdenum(V)

C. Balagopalakrishna, John T. Kimbrough, and T. David Westmoreland*

Department of Chemistry, Wesleyan University, Middletown, Connecticut 06459

Received September 1, 1995[⊗]

The EPR spectroscopic parameters of a series of Mo(V) oxyhalide anions, $[MoOX_{5-n}(H_2O)_n]^{(2-n)-}$ (X = F, Br, $n = 0$; X = Cl, $n = 1$), were obtained in fluid solutions and frozen glasses or (X = Cl, Br) doped into single crystals of a diamagnetic host lattice. The electronic structures of the complexes were approximated by optimizing the electronic structural parameters of a LCAO model to reproduce the experimentally observed EPR parameters. The results indicate quantitatively that the most important contribution to deviations from $g = g_e$ in the complexes is metal−ligand covalency. Charge transfer excited state mixing and ligand spin−orbit coupling (for X = Cl, Br) provide significant but smaller contributions to the EPR parameters. The isotropic molybdenum hyperfine coupling constants are also shown to be dominated by Fermi contact interactions. A number of implications with respect to the EPR spectroscopy of molybdenum oxidoreductases are noted. The crystal and molecular structure of a diamagnetic Nb(V) lattice is also reported. $(H_2dafone)[NbOCl_4(H_2O)]Cl$ (dafone = 4,5-diazafluoren-9-one) crystallizes in the monoclinic space group $C2/c$ with $a = 16.0043(2)$ Å, $b = 24.8021(3)$ Å, $c = 10.0162(2)$ Å, $\beta = 121.048(1)°$, and $Z = 8$.

Introduction

The electronic structures of complexes containing the molybdenyl ($\{MoO\}^{3+}$) group continue to be of interest due largely to their relevance to the active sites of molybdenum oxidoreductase enzymes.[1−8] Molybdenum-containing oxidoreductase enzymes are nearly ubiquitous in biological systems and exhibit several common structural and chemical features. They are all based on an active site that contains a single molybdenum atom associated with a pterin-based cofactor which is postulated to bind to molybdenum as a 1,2-dithiolene chelate.[9] This proposal has recently been confirmed crystallographically for the molybdenum-containing aldehyde oxidoreductase from *D. gigas*.[10] The principal substrate binds at the molybdenum site and the metal cycles between the +6 and +4 oxidation states during catalysis. The reactions catalyzed by the molybdenum oxidoreductases formally correspond to oxygen atom transfers and include organic hydroxylations,[11−13] inorganic oxidations,[11,12] and inorganic reductions.[11,14] Each enzyme (except some bacterial dimethyl sulfoxide (DMSO) reductases[11,15]) contains other prosthetic groups which are involved in one electron transfer reactions with external electron acceptors or donors that complete the net catalytic cycle. It is through these sites that two outer sphere one-electron redox steps are coupled to a net two-electron transfer reaction at the molybdenum site.

Given the importance of these enzymes to an array of biological processes, a clearer understanding of the relationships between their active site structures and catalytic mechanisms is needed. Unfortunately, only one crystallographic structure is available for any molybdenum oxidoreductase,[10] and the current pictures of most of the active sites are based almost exclusively on spectroscopic evidence. In particular, the combined results of extended X-ray absorption fine structure (EXAFS) spectroscopy and electron paramagnetic resonance (EPR) spectroscopy have led to specific structural proposals for several forms of the enzyme active sites which appear during the catalytic cycle. EXAFS spectroscopy has provided the most direct insight into the structural details of the immediate coordination sphere of molybdenum in the fully oxidized and reduced forms of the enzyme.[16−20] These studies indicate that the fully oxidized Mo(VI) forms of each enzyme contain either two terminal oxo groups or, for xanthine oxidase, terminal oxo and sulfido. The reduced Mo(IV) forms exhibit significant

[⊗] Abstract published in *Advance ACS Abstracts,* October 15, 1996.

(1) *Molybdenum and Molybdenum Containing Enzymes;* Coughlan, M., Ed.; Pergamon: New York, 1980.
(2) *Molybdenum Enzymes*; Spiro, T. G., Ed.; Wiley-Interscience: New York, 1985.
(3) *Molybdenum Enzymes, Cofactors, and Model Systems*; Steifel, E. I., Coucouvanis, D., Newton, W. E., Eds.; ACS Symposium Series 535; American Chemical Society: Washington, D. C., 1993.
(4) Steifel, E. I. *Prog. Inorg. Chem.* **1977**, *22*, 1−223.
(5) Burgmayer, S. J. N.; Steifel, E. I. *J. Chem. Educ.* **1985**, *62*, 943−953.
(6) Bray, R. C. *Q. Rev. Biophys.* **1988**, *21*, 299−329.
(7) Wooton, J. C.; Nicolson, R. E.; Cock, J. M.; Walters, D. E.; Burke, J. F.; Doyle, W. A.; Bray, R. C. *Biochem. Biophys. Acta* **1991**, *1057*, 157−185.
(8) Enemark, J. H.; Young, C. G. *Adv. Inorg. Chem.* **1993**, *40*, 1−88.
(9) (a) Johnson, J. L.; Hainline, B. E.; Rajagopalan, K. V. *J. Biol. Chem.* **1980**, *255*, 1783−1786. (b) Rajagopalan, K. V.; Johnson, J. L. *J. Biol. Chem.* **1992**, *267*, 10199−10202. (c) Rajagopalan, K. V. In Ref 3; pp 38−49.
(10) Romão, M. J.; Archer, M., Moura, I.; Moura, J.; LeGall, J.; Engh, R.; Schneider, M.; Hof, P.; Huber, R. *Science* **1995**, *270*, 1170−1176.
(11) Steifel, E. I. In Ref 3; pp 1−19, and references cited therein.
(12) Hille, R; Massey, V. In ref 2, pp. 443−518.
(13) Hille, R. In *Chemistry and Biochemistry of Flavoenzymes*; Müller, F., Ed.; CRC Press: Boca Raton, FL, 1992; Vol. III, pp 21−68.
(14) (a) Adams, M. W. W.; Mortenson, L. E. In Ref 2, pp 519−593. (b) Barber, M. J.; Solomonson, L. P. In *Chemistry and Biochemistry of Flavoenzymes*; Müller, F., Ed.; CRC Press: Boca Raton, FL, 1992; Vol. III, pp 319−331.
(15) (a) Satoh, T.; Kurihara, F. N. *J. Biochem. (Tokyo)* **1987**, *102*, 191−197. (b) Bastian, N. R.; Kay, C. J.; Barber, M. J.; Rajagopalan, R. V. *J. Biol. Chem.* **1991**, *266*, 45−51. (c) McEwan, A. G.; Ferguson, S. J.; Jackson, J. B. *Biochem. J.* **1991**, *274*, 305−307.
(16) (a) Cramer, S. P. *Adv. Inorg. Bioinorg. Mech.* **1983**, *2*, 259−316. (b) Cramer, S. P. *Chem. Anal. (N. Y.)* **1988**, *92*, 257−320.
(17) (a) Cramer, S. P.; Wahl, R.; Rajagopalan, K. V. *J. Am. Chem. Soc.* **1981**, *103*, 7721−7727. (b) Cramer, S. P.; Hille, R. *J. Am. Chem. Soc.* **1985**, *107*, 8164−8169. (c) Turner, N. A.; Bray, R. C.; Diakun, G. P. *Biochem. J.* **1989**, *260*, 563−571.
(18) George, G. N.; Kipke, C. A.; Prince, R. C.; Sunde, R. A.; Enemark, J. H.; Cramer, S. P. *Biochemistry* **1989**, *28*, 5075−5080.
(19) George, G. N.; Cleland, W. E., Jr.; Enemark, J. H.; Smith, B. E.; Kipke, C. A.; Roberts, S. A.; Cramer, S. P. *J. Am. Chem. Soc.* **1990**, *112*, 2541−2548.

S0020-1669(95)01142-6 CCC: $12.00

Table 1. EPR Parameters of Representative Molybdenum Oxidoreductase Sites

species	g_1	g_2	g_3	selected hyperfine coupling constants[a]	refs
xanthine oxidase:					16a, 21, 22
very rapid	2.025	1.955	1.949	27.2 (^{95}Mo); 11.5 (33S)	
rapid type 1	1.989	1.969	1.965	37.1 (^{95}Mo); 3.3 (33S); 12.5, 2.8 (^{1}H)	
slow	1.971	1.966	1.954	39.6 (^{95}Mo); 14.6, 1.6 (^{1}H)	
sulfite oxidase:					16a, 18, 23
high pH	1.987	1.964	1.953	12 (^{17}O)	
low pH	2.004	1.972	1.966	32.8 (^{95,97}Mo); 9.1 (^{1}H); 6 (^{17}O)	
nitrate reductase:					16a, 24
signal A	1.996	1.969	1.967	1.25 (^{1}H)	
signal B	1.996	1.969	1.967		

[a] Hyperfine coupling constants are given in units of 10^{-4} cm^{-1} and represent the average value of A_1, A_2, and A_3.

changes in bond lengths. The additional observation of ^{1}H splittings in the EPR spectra of Mo(V) derivatives of the sites suggests that the bond length changes are associated with protonation of one of the terminal groups. The EXAFS spectra are also consistent with coordination by the proposed dithiolene cofactor, but the nature of any other ligands to molybdenum has not yet been defined.

A major contribution to the current understanding of the structures of molybdenum oxidoreductase active sites has come from EPR spectroscopy. Partial reduction of native enzymes or treatment of the enzymes with some inhibitors produces Mo(V) species with one unpaired electron ($S = {}^1/_2$). These species give EPR signals in the $g \approx 2$ region, and many such signals have been characterized in terms of g values and the hyperfine coupling constants which arise from coupling of the electronic spin to nuclei of nonzero spin.[6,15b,16a,21−25] Representative EPR parameters that have been obtained for Mo(V) species in the enzymes are collected in Table 1.

A very curious feature of these parameters is that, for some of the sites, one of the g values is greater than g_e (=2.0023). Simple ligand field models[26−29] for d^1 systems in axial symmetry predict that the g values should exhibit the relative magnitudes

$$g_e > g_\perp (=g_{x,y}) > g_\parallel (=g_z)$$

Similar anomalous trends in g values have been observed in many model systems. A few representative examples are given in Table 2. The anomalously high g values ($g_\parallel > g_e$) and the "inverted" trend $g_\parallel > g_\perp$ observed in some enzyme sites (e.g., very rapid xanthine oxidase) and model complexes (e.g., $[MoO(SPh)]_4^-$) have often been qualitatively attributed[29−31,36−45]

Table 2. EPR Parameters of Selected Mo(V) Complexes[a,b]

complex	g_1	g_2	g_3	g_{iso}	A_{iso}^{Mo}	ref
$[MoO(SPh)_4]^-$	2.017	1.979	1.979	1.990	32.3	30, 31
$[MoO(SePh)_4]^-$	2.072	2.005	2.005	2.024	30.0	31
$[MoOL]^+$	2.0020	1.9560	1.9445	1.9670	37.6	32
$[MoO_2L]^-$	1.9855	1.9121	1.8112	1.9007	43.9	32
$[MoOSL]^-$	2.0165	1.9330	1.8885	1.9435	37.2	32
cis-MoO(OH)L	1.9805	1.9470	1.9440	1.9570	40.2	32
cis-MoO(SH)L	2.0160	1.9610	1.9535	1.9765	35.1	32
$Tp^*MoO(OPh)_2$	1.959	1.938	1.901	1.932	44.2	33
$Tp^*MoO(SPh)_2$	2.004	1.950	1.937	1.967	35.8	33
Tp^*MoOF_2	1.977	1.920	1.904	1.9331	51.0	34
Tp^*MoOCl_2	1.971	1.941	1.934	1.947	46.0	33, 35
Tp^*MoOBr_2	2.042	1.94	1.94	1.9746	43.4	34
Tp^*MoSCl_2	1.921	1.941	1.919	1.928	46.8	36

[a] Hyperfine coupling constants are in units of 10^{-4} cm^{-1}. [b] Abbreviations: L = *N*,*N*′-dimethyl-*N*,*N*′-bis(2-mercaptophenyl)ethylenediamine dianion; Tp* = hydrotris(3,5- dimethylpyrazol-1-yl)borate anion.

to various combinations of three effects: (1) large metal−ligand covalencies, (2) large values of ligand spin−orbit coupling, and (3) the influence of low-energy charge transfer states. These proposals have not, however, been quantitatively evaluated to determine the relative importance of these effects. If, for example, the g values are determined primarily by metal−ligand covalency, then a quantitative electronic structural model would

(20) (a) Cramer, S. P.; Solomonson, L. P.; Adams, M. W. W.; Mortenson, L. E. *J. Am. Chem. Soc.* **1984**, *106*, 1467−1471. (b) George, G. N.; Turner, N. A.; Bray, R. C.; Morpeth, F. F.; Boxer, D. H. *Biochem. J.* **1989**, *259*, 693−700.
(21) George, G. N.; Bray, R. C. *Biochemistry* **1988**, *27*, 3603−3609.
(22) Wilson, G. L.; Greenwood, R. J.; Pilbrow, J. R.; Spence, J. T.; Wedd, A. G. *J. Am. Chem. Soc.* **1991**, *113*, 6803−6812.
(23) Dhawan, I. K.; Pacheco, A.; Enemark, J. H. *J. Am. Chem. Soc.* **1994**, *116*, 7911−7912.
(24) (a) Gutteridge, S.; Bray, R. C.; Notton, B. A.; Fido, R. J.; Hewitt, E. J. *Biochem. J.* **1983**, *213*, 137−142. (b) Solomonson, L. P.; Barber, M. J.; Howard, W. D.; Johnson, J. L.; Rajagopalan, K. V. *J. Biol. Chem.* **1984**, *259*, 849−853. (c) Kay, C. J.; Barber, M. J. *Biochemistry* **1989**, *28*, 5750−5758.
(25) (a) Bray, R. C.; George, G. N.; Gutteridge, S.; Norlander, L.; Stell, J. G. P.; Stubley, C. *Biochem. J.* **1982**, *203*, 263−267. (b) Barber, M. J.; Coughlan, M. P.; Rajagopalan, K. V.; Siegel, L. M. *Biochemistry* **1982**, *21*, 3561−3568.
(26) McGarvey, B. R. In *Transition Metal Chemistry*; Carlin, R. L., Ed.; Marcel Dekker: New York, 1966; Vol. 3, pp 89−201.
(27) Bencini, A.; Gatteschi, D. In *Transition Metal Chemistry*; Melson, G. A., Figgis, B. N., Eds.; Marcel Dekker: New York, 1982; Vol. 8, pp 1−178.
(28) Solomon, E. I. *Comments Inorg. Chem.* **1984**, *3*, 225−320.
(29) Mabbs, F. E.; Collison, D. *Electron Paramagnetic Resonance of d Transition Metal Compounds*; Elsevier: Amsterdam, 1992.
(30) Boyd, I. W.; Dance, I. G.; Murray, K. S.; Wedd, A. G. *Aust. J. Chem.* **1978**, *31*, 279−284.
(31) Hanson, G. R.; Brunette, A. A.; McDonell, A. C.; Murray, K. S.; Wedd, A. G. *J. Am. Chem. Soc.* **1981**, *103*, 1953−1959.
(32) Dowerah, D.; Spence, J. T.; Singh, R.; Wedd, A. G.; Wilson, G. L.; Farchione, F.; Enemark, J. H.; Kristofzski, J.; Bruck, M. *J. Am. Chem. Soc.* **1987**, *109*, 5655−5665.
(33) Cleland, W. E., Jr.; Barnhart, K. M.; Yamanouchi, K.; Collison, D.; Mabbs, F. E.; Ortega, R. B.; Enemark, J. H. *Inorg. Chem.* **1987**, *26*, 1017−1025.
(34) Nipales, N. S.; Westmoreland, T. D. *Inorg. Chem.* **1995**, *34*, 3374−3377.
(35) (a) Collison, D.; Mabbs, F. E.; Enemark, J. H.; Cleland, W. E., Jr. *Polyhedron* **1986**, *5*, 423−425. (b) Collison, D.; Eardley, D. R.; Mabbs, F. E.; Rigby, K.; Enemark, J. H. *Polyhedron* **1989**, *8*, 1833−1834.
(36) Young, C. G.; Enemark. J. H.; Collison, D.; Mabbs, F. E. *Inorg. Chem.* **1987**, *26*, 2925−2927.
(37) DeArmond, K.; Garrett, B. B.; Gutowsky, H. S. *J. Chem. Phys.* **1965**, *42*, 1019−1025.
(38) Kon, H.; Sharpless, N. E. *J. Phys. Chem.* **1966**, *70*, 105−111.
(39) Manoharan, P. T.; Rogers, M. T. *J. Chem. Phys.* **1968**, *49*, 5510−5519.
(40) Lee, G. R.; Spence, J. T. *Inorg. Chem.* **1972**, *11*, 2354−2356.
(41) (a) Radhakrishna, S.; Chowdari, B. V. R.; Viswanath, A. K. *Chem Phys. Lett.* **1975**, *30*, 231−234. (b) Radhakrishna, S.; Chowdari, B. V. R.; Viswanath, A. K. *Chem. Phys. Lett.* **1976**, *42*, 319−322.
(42) Sunil, K. K.; Harrison, J. F.; Rogers, M. T. *J. Chem. Phys.* **1982**, *76*, 3087−3097.
(43) (a) Chang, C. S. J.; Collison, D.; Mabbs, F. E.; Enemark, J. H. *Inorg. Chem.* **1990**, *29*, 2261−2267. (b) Chang, C. S. J.; Enemark, J. H. *Inorg. Chem.* **1991**, *30*, 683−688.
(44) Collison, D.; Eardley, D. R.; Mabbs, F. E.; Rigby, K., Bruck, M. A.; Enemark, J. H.; Wexler, P. A. *J. Chem. Soc., Dalton Trans.* **1994**, 1003−1011.
(45) Sabel, D. M.; Gewirth, A. A. *Inorg. Chem.*, **1994**, *33*, 148−156.

provide valuable correlations between the observed EPR spectra and the bonding in the site. The species listed in Table 1 also exhibit a variety of metal and ligand hyperfine couplings, particularly to protons. However, little is understood in detail about how these EPR parameters reflect the specific active site electronic structures and coordination geometries. It would be useful to understand in more detail how the electronic structure is manifested in the EPR spectroscopic parameters.

We have begun to develop a methodology for relating Mo(V) EPR parameters to electronic structure and thence to specific features of the coordination geometry. Such correlations may provide a basis for quantitative interpretation of the EPR spectra of the molybdenum oxidoreductase signals as well as significant new insights into the mechanisms of catalysis. We report herein the results of our initial efforts on oxyhalide complexes of Mo(V), a series of relatively simple species of high symmetry for which many analogues containing other metals are known. A number of previous studies have addressed the EPR[37−39,41,46−50] and optical[45,49−53] spectroscopies of these species. We have fully defined, *via* oriented single crystal EPR spectroscopy, the EPR parameters of the tetragonal $[MoOCl_4(H_2O)]^-$ and $[MoOBr_5]^{2-}$ anions. A relatively simple LCAO model for these systems and for $[MoOF_5]^{2-}$ has been employed in an optimization procedure which exactly reproduces the observed g values and A^{Mo} constants to within the experimental error. The detailed quantitative picture which emerges provides insight into the origin of the anomalous EPR parameters of the enzyme active sites and model complexes.

Experimental Section

Synthesis. All materials were obtained commercially and used as received except as noted below. Elemental analyses were performed by Atlantic Microlabs. Dafone (4,5-diazafluoren-9-one) was prepared according to the published synthesis.[54]

Cs_2MoOF_5. The complex salt was prepared by a modification of the reported method for the potassium salt.[39] A 1.37 g portion of $MoCl_5$ was dissolved in 30 mL of 48% aqueous HF in a polyethylene beaker. To the blue solution was added 0.8 g of CsF in 30 mL of 48% HF, and the mixture was allowed to stand overnight. Cs_2MoOF_5 precipitated as greenish-blue needles.

$(H_2dafone)[MoOCl_4(H_2O)]Cl$. The anion $[MoOCl_4(H_2O)]^-$ was obtained by a modification of the reported procedure.[55] A 0.0806 g (0.5 mmol) sample of MoO_3 in a mixture of 15 mL of concentrated HCl with 2 mL of HI (5.5 M) was boiled until the solution was reduced to a volume of 5 mL. Repeated additions of concentrated HCl were made until a bright green solution resulted. To this hot solution, a hot HCl solution of dafone (0.1239 g, 0.68 mmol) was added, and the heating was stopped immediately. On cooling to room temperature, large yellowish-green plates separated from the solution. The crystals were filtered and dried over KOH under vacuum. The formulation of the crystals is based on the elemental analysis and the previous observation that $[MoOCl_4(H_2O)]^-$ is the predominant anionic form of Mo(V) under these conditions.[56] Yield: 0.261 g (98%). Anal. Calcd for $C_{11}H_{10}N_2O_3MoCl_5$ (%): C, 26.89; H, 2.05; N, 5.70; Cl, 36.07. Found (%): C, 28.06; H, 2.03; N, 5.83; Cl, 36.06. IR (cm^{-1}): ν(C═O), 1751; ν(Mo═O), 989.

$(H_2dafone)[NbOCl_4(H_2O)]Cl$. $NbCl_5$ (0.270 g, 0.1 mmol) was dissolved in 15 mL of concentrated HCl and placed in a long cylindrical flat bottomed column (approximately 45 × 1.25 cm). A layer of concentrated HCl was added, followed by a solution of dafone (0.1821 g, 0.1 mmol) in 5 mL of concentrated HCl. These solutions were allowed to diffuse together, and needles formed overnight. The mixture was filtered, and X-ray quality colorless crystals of $(H_2dafone)[NbOCl_4(H_2O)]Cl$ were obtained by slow evaporation of the filtrate over concentrated H_2SO_4 in a desiccator. The identity of the complex was confirmed by the X-ray crystallographic results presented below. IR (cm^{-1}): ν(C═O), 1736; ν(Nb═O), 908.

Doped Single Crystals, $(H_2dafone)[Nb\{Mo\}OCl_4(H_2O)]Cl$. Mo-doped single crystals were obtained by mixing concentrated HCl solutions of dafone (0.1239 g, 0.68 mmol) and $NbCl_5$ (0.2522g, 0.93 mmol) with a small amount of a solution of $MoOCl_4(H_2O)^-$. The mixture was filtered, and the filtrate was allowed to evaporate at room temperature over concentrated H_2SO_4, yielding large yellowish-green crystals. The crystals were dried over KOH and used for the spectroscopic experiments described below.

$(Bu_4N)_2[SnBr_6]$ and $(Bu_4N)_2[SnBr_6\{MoOBr_5\}]$. The complex $(Bu_4N)_2[SnBr_6]$ was obtained as large cubes by a procedure analogous to the published synthesis of $(NH_4)_2[SnBr_6]$[47c] involving a slow diffusion together of solutions of Bu_4NBr (0.3224 g, 1 mmol) and $SnBr_4$ (0.2192 g, 0.5 mmol) in concentrated HBr. Colorless crystals separated over a period of 2 weeks to give a yield of 0.3783 g (68%). Anal. Calcd for $C_{32}H_{72}N_2SnBr_6$ (%): C, 35.49; H, 6.70; N, 2.59; Br, 44.27. Found (%): C, 35.54; H, 6.80; N, 2.67; Br, 44.27. The Mo-doped crystals were obtained similarly by adding a small amount of a solution of $[MoOBr_{5-n}(H_2O)_n]^{(2-n)-}$ (prepared by reduction of MoO_3 in concentrated HBr analogously to the chloro complex) to the $SnBr_4$ solution before addition of the Bu_4NBr solution. The value of n in the formula of the species doped into the lattice is not entirely clear, but a number of arguments suggest that $n = 5$. It is, for example, known that $[MoOBr_5]^{2-}$ is the dominant oxyhalide species in 9.4 M HBr[57] and that the shape and charge of the pentahalide anion are most similar to those of the anion of the host lattice. Also, as noted below, the measured EPR parameters compare quite well with the published values[47c,48,57] for the $[MoOBr_5]^{2-}$ anion.

X-ray Structure Determination for $(H_2dafone)[NbOCl_4(H_2O)]Cl$. The X-ray data collection and structure solution were conducted by Dr. V. G. Young, Jr., of the X-Ray Crystallographic Center at The University of Minnesota. All calculations were performed using the SHELXTL V5.0 suite of programs. A suitable crystal of $(H_2dafone)[NbOCl_4(H_2O)]Cl$, obtained as described above, was mounted on a glass fiber. Data were collected at 173 K on a Siemens SMART system. An initial set of cell constants was calculated from the reflections for three sets of 30 frames. Final cell constants were calculated from a set of strong reflections from the collected data set.

The space group $C2/c$ was determined on the basis of systematic absences and intensity statistics. A successful direct-methods solution was calculated which provided most non-hydrogen atoms from the E-map. Full-matrix least squares/difference Fourier cycles located the remainder of the non-hydrogen atoms. All non-hydrogen atoms were refined with anisotropic displacement parameters. The water hydrogens were refined isotropically with similar distance restraints to the host oxygen atom and with the isotropic displacement parameter fixed at 1.5 times that of the host oxygen atom. Full-matrix least-squares refinement with 216 parameters, using 2981 reflections, led to convergence with $R = 0.0480$ ($I \geq 2\sigma(I)$) or $R = 0.0535$ (all data). Additional collection and refinement details are given in the Supporting Information.

(46) Hare, C. R.; Bernal, I.; Gray, H. B. *Inorg. Chem.* **1962**, *1*, 831−835.
(47) (a) van Kemenade, J. T. C.; Verbeek, J. L.; Cornaz, P. F. *Recl. Trav. Chim. Pays-Bas* **1966**, *85*, 629−630. (b) van Kemenade, J. T. C. *Recl. Trav. Chim. Pays-Bas* **1970**, *89*, 1100−1108. (c) van Kemenade, J. T. C. *Recl. Trav. Chim. Pays-Bas* **1973**, *92*, 1102−1120.
(48) Dalton, L. A.; Bereman, R. D.; Brubaker, C. H., Jr. *Inorg. Chem.* **1969**, *8*, 2477−2480.
(49) (a) Garner, C. D.; Hill, L. H.; Mabbs, F. E.; McFadden, D. L.; McPhail, A. T. *J. Chem. Soc., Dalton Trans.* **1977**, 853−858. (b) Garner, C. D.; Hill, L. H.; Mabbs, F. E.; McFadden, D. L.; McPhail, A. T. *J. Chem. Soc., Dalton Trans.* **1977**, 1202−1207.
(50) Scullane, M. I.; Taylor, R. D.; Minelli, M.; Spence, J. T.; Yamanouchi, K.; Enemark, J. H.; Chasteen, N. D. *Inorg. Chem.* **1979**, *18*, 3213−3219.
(51) (a) Gray, H. B.; Hare, C. R. *Inorg. Chem.* **1962**, *1*, 363−368. (b) Winkler, J. R.; Gray, H. B. *Comments Inorg. Chem.* **1981**, *1*, 257−263.
(52) Collison, D. *J. Chem. Soc., Dalton Trans.* **1990**, 2999−3006.
(53) Carducci, M. D.; Brown, C.; Solomon, E. I.; Enemark J. H. *J. Am. Chem. Soc.* **1994**, *116*, 11856−11868.
(54) Henderson, L. J., Jr.; Fronczek, F. R.; Cherry, W. R. *J. Am. Chem. Soc.* **1984**, *106*, 5876−5879.
(55) Saha, H. K.; Haldar, M. C. *Inorg. Synth.* **1979**, *19*, 134−136.
(56) Boorman, P. M.; Garner, C. D.; Mabbs, F. E. *J. Chem. Soc., Dalton Trans.* **1975**, 1299−1306.
(57) Dowsing, R. D.; Gibson, J. F. *J. Chem. Soc. A* **1967**, 655−660.

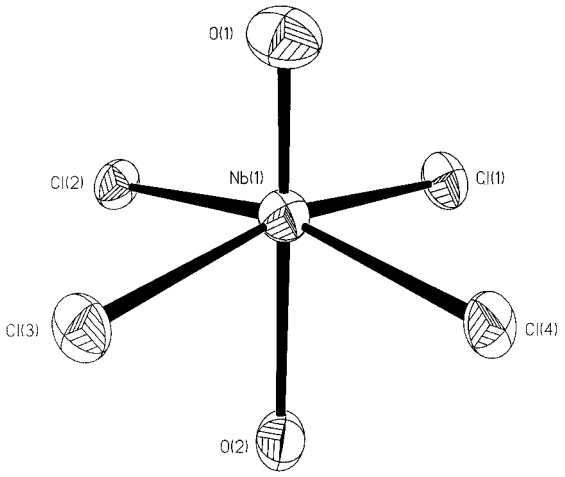

Figure 1. ORTEP plot of the $[NbOCl_4(H_2O)]^-$ anion. Selected bond distances (Å) and angles (deg): Nb(1)—O(1), 1.700(4), Nb(1)—O(2),2.342(4); Nb(1)—Cl(1), 2.4184(13); Nb(1)—Cl(2), 2.4436(12); Nb(1)—Cl(3), 2.4277(13); Nb(1)—Cl(4), 2.4384(12); O(1)—Nb(1)—O(2), 177.8(2); O(1)—Nb(1)—Cl(1), 97.8(2); O(1)—Nb(1)—Cl(2), 98.2(2); O(1)—Nb(1)—Cl(3), 97.5(2); O(1)—Nb(1)—Cl(4), 97.3(2); Cl(1)—Nb(1)—Cl(2), 88.65(5); Cl(2)—Nb(1)—Cl(3), 87.98(5); Cl(3)—Nb(1)—Cl(4), 90.89(5); Cl(1)—Nb(1)—Cl(4), 88.40(5).

EPR Spectroscopy. X-band EPR spectra were obtained with a Bruker ESP-300 spectrometer in a TE_{102} rectangular cavity. Q-band data were obtained at Bruker Instruments, Billerica, MA, on a similar instrument. A 100 KHz modulation was used for observing the first derivative signal. The reported spectra are typically an average of 25 scans. For spectra of concentrated aqueous acid solutions, the samples were loaded into lengths of flattened 1 mm Teflon tubing which had been mechanically sealed at one end. The Teflon tubes were then inserted into conventional quartz sample tubes for measurements. This method approximates a standard flat cell but avoids the corrosive effects of strong acids (especially HF) on the sample tube.

For oriented measurements, single crystals were mounted on quartz rods with silicone grease. Spectra were recorded for every 10° change in orientation of the magnetic field vector with respect to the plane under study. The EPR interaction matrices were obtained by recording the angular dependence of the signals in three mutually perpendicular planes, taking care that the *g* and *A* values exactly matched when the magnetic field was along a direction common to two planes. At each orientation, the EPR signals were an average of 50 scans. The spectrometer frequency at each orientation was measured with a Hewlett-Packard 5255A frequency counter.

Results

Molecular and Crystal Structure of $(H_2dafone)[NbOCl_4(H_2O)]Cl$. $(H_2dafone)[NbOCl_4(H_2O)]Cl$ crystallizes in the monoclinic space group $C2/c$ with $Z = 8$ and one $[NbOCl_4(H_2O)]^-$ anion per asymmetric unit. The dafone ligand in the lattice is doubly protonated, and there is a chloride ion in the lattice which forms a number of hydrogen bonds to NH protons of $[H_2dafone]^{2+}$ as well as to the aquo ligand of $[NbOCl_4(H_2O)]^-$. Figure 1 illustrates the geometry about niobium in the anion. The anion effectively has C_{4v} point group symmetry with the Nb—O(1) bond along the 4-fold rotation axis. The structural parameters of the anion are very similar to those of the $[MoOCl_4(H_2O)]^-$ anion previously characterized as the tetraphenylarsonium salt.[49b] Complete tables of bond distances and angles are given in the Supporting Information.

Figure 2 shows the full unit cell of $(H_2dafone)[NbOCl_4(H_2O)]Cl$. Of particular interest are the relative orientations of the anions in the cell. For a given anion, three other anions in the cell are related by translations and/or inversions and are therefore magnetically equivalent and their EPR spectra have identical orientation dependencies. The other four anions are obtained by 2-fold rotations of the first four. These four sites, while magnetically equivalent to each other, are inequivalent to the other four sites and may have a different orientation of their *g* and *A* interaction matrices with respect to the crystallographic axes. As is evident from the atomic coordinates, the Nb—O axes in each site are only 2.132° from the *a* axis and thus make an angle of 4.3° with respect to each other. The EPR interaction matrices have very nearly the same orientations for the two types of sites, and the EPR data presented below do not resolve the features of each site. In the subsequent analysis the parameters are treated as originating from a single site.

Solution and Powder Spectra. The EPR spectra of Mo(V) oxyhalide anions in concentrated aqueous acid solutions at 298 and 77 K are shown in Figure 3. Clearly apparent in each solution spectrum are the central signal from the ions containing ^{98}Mo ($I_N = 0$, 75% natural abundance) and the sextet from the

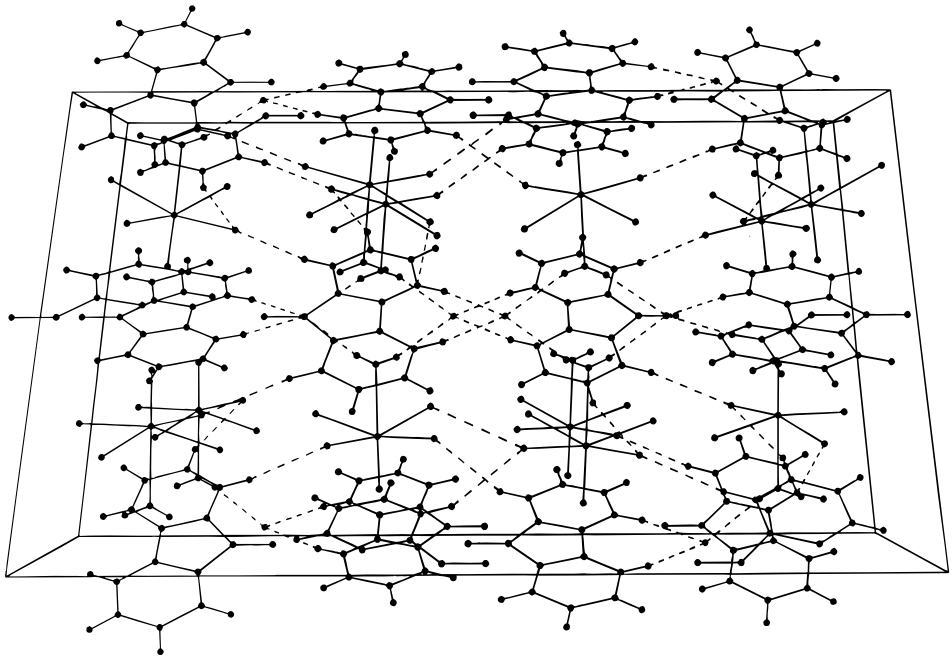

Figure 2. Schematic view of one unit cell of $(H_2dafone)[NbOCl_4(H_2O)]Cl$. The view is approximately along the c^* direction with the *a* axis vertical and the *b* axis horizontal. Hydrogen bonding interactions are denoted by dashed lines.

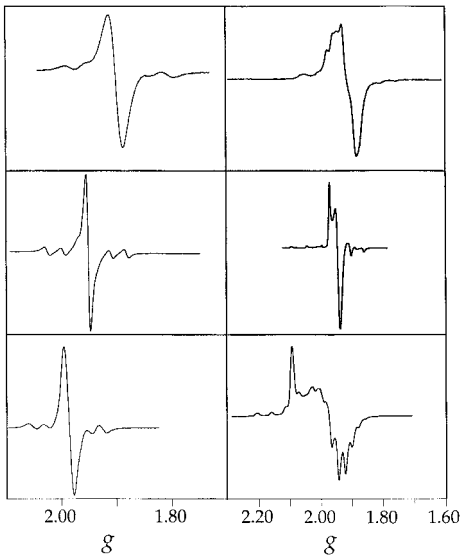

Figure 3. Room temperature (left) and 77 K frozen solution (right) X-band EPR spectra of $[MoOF_5]^{2-}$ (top), $[MoOCl_4(H_2O)]^-$ (middle), and $[MoOBr_5]^{2-}$ (bottom).

Table 3. Experimentally Determined EPR Parameters for Mo(V) Oxyhalide Complexes, $[MoOX_{5-n}(H_2O)_n]^{(2-n)-}$ ($n = 0$ or 1)[a,b]

	X = F	X = Cl	X = Br
g_{iso}	1.902	1.944	1.985
A_{iso}^{Mo}	68.0	45.0	44.0
$g_{\|\|}$	1.894[c]	1.9632[d]	2.090[e]
$g_\perp$	1.913[c]	1.9400[d]	1.945[e]
$\langle g \rangle$	1.907	1.948	1.993
$A_{\|\|}^{Mo}$	90.1[c]	74.7[d]	66.0[e]
$A_\perp^{Mo}$	42.5[c]	32.6[d]	33.0[f]
$\langle A^{Mo} \rangle$	58.4	46.6	44.0

[a] Hyperfine constants are in units of 10^{-4} cm^{-1}. [b] Isotropic parameters are from the room temperature data in Figure 3. [c] From ref 47b. [d] From the oriented single crystal analysis of $(H_2dafone)[Nb\{Mo\}OCl_4(H_2O)]Cl$. [e] From the oriented single crystal analysis of $(Bu_4N)_2[SnBr_6\{MoOBr_5\}]$. [f] Calculated from A_{iso}^{Mo} and $A_{||}^{Mo}$.

^{95,97}Mo containing ions ($I_N = {}^5/_2$, 25% combined natural abundance). The resulting isotropic parameters g_{iso}, and A_{iso}^{Mo} for each complex are collected in Table 3. A significant trend is the increase of g_{iso} values and decrease of A_{iso}^{Mo} from the fluoride to the bromide. The EPR spectra of the frozen acid solutions at 77 K are complex, and only the features associated with the $g_{||}$ region are clearly resolved. The extensive halide superhyperfine coupling from fluorine and bromine was not further analyzed. No resolved superhyperfine structure due to ^{35,37}Cl was observed in solutions, powders, or single crystals at any temperature.

Oriented Single Crystal Spectra. For $(H_2dafone)[Nb\{Mo\}OCl_4(H_2O)]Cl$, the angular variations of g^2 and $(gA^{Mo})^2$ in three mutually perpendicular planes of a single crystal are shown in Figure 4. As noted above, only one set of signals is resolved at all orientations. Representative EPR spectra with the magnetic field parallel to and perpendicular to the crystallographic *a* axis are shown in Figure 5.

The experimental *g* values in each plane were fit by standard least-squares methods to the models of Waller and Rogers.[58] Diagonalization of the resulting $\mathbf{g}^2$ tensor gave the principal values of the **g** matrix as the square roots of the diagonal elements. The molybdenum hyperfine interaction matrix was determined by an analogous procedure.[58,59] The principal values

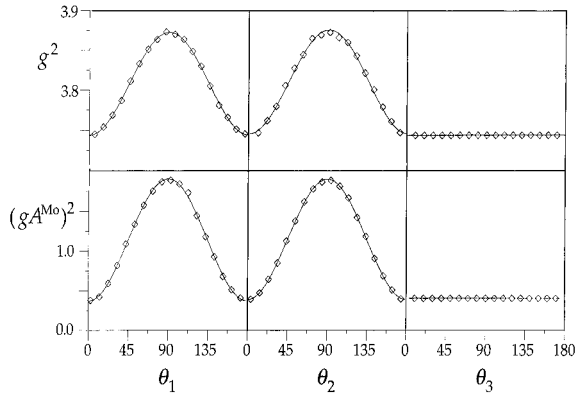

Figure 4. Angular variation of g^2 and $(gA^{Mo})^2$ values of $(H_2dafone)[Nb\{Mo\}OCl_4(H_2O)]Cl$ for rotations of **B** in three mutually perpendicular planes: *ac** (left), *ab* (middle), and *bc** (right). The *b* axis was identified from the angular dependence of the extinctions of plane polarized light in the crystal under crossed polarizers. The *a* axis was assigned on the basis of the unit cell dimensions and the crystal dimensions.

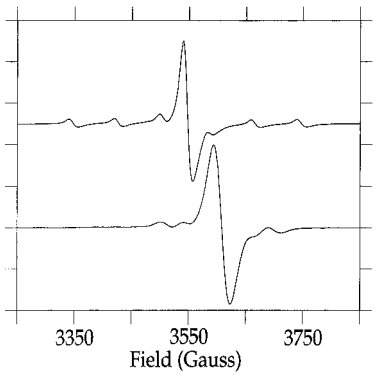

Figure 5. Limiting orientation EPR spectra of $(H_2dafone)[Nb\{Mo\}OCl_4(H_2O)]Cl$. Upper: **B** parallel to *a*. Lower: **B** perpendicular to *a*.

confirm the axial symmetry of the **g** and **A** interaction matrices as well as the collinearity of the *g* and *A* principal axes as required by the C_{4v} symmetry of the ion.

Attempts to grow large single crystals of $(H_2dafone)[Nb\{Mo\}OBr_4(H_2O)]Br$ were unsuccessful, and only powders were obtained. It was, however, possible to dope $[MoOBr_5]^{2-}$ into a lattice of $(Bu_4N)_2[SnBr_6]$. The X-band single crystal EPR spectrum of $[MoOBr_5]^{2-}$ doped into the $(Bu_4N)_2[SnBr_6]$ lattice is extremely complex, even at 115 K, due to overlapping metal and ligand hyperfine features. In addition, there are multiple sites which contribute to the spectrum. The angular dependencies of the EPR spectra indicate that the orientation of the Mo—O axis in the doped crystals is statistically disordered over the three orthogonal axes of the $[SnBr_6]^{2-}$ group since at a general orientation of the applied field three different overlapping spectra are observed. Experimental determination of the principal values of *g* and A^{Mo} was therefore difficult at X-band. The parallel and perpendicular regions of the spectrum of the crystal were, however, resolved at Q-band at 298 K. Figure 6 shows the spectrum at an orientation along one of the orthogonal crystallographic axes at which the signals were well-resolved. As is evident from the figure, the ligand superhyperfine structure is not resolved at Q-band and thus does not interfere with the determination of $g_\perp$. This spectrum represents the first direct experimental determination of $g_\perp$ for $[MoOBr_5]^{2-}$. All attempts to dope $[MoOF_5]^{2-}$ into a suitable host lattice were unsuccessful. For the purposes of the analysis, we have therefore relied on single crystal EPR parameters which have been previously published.[47b]

(58) Waller, W. G.; Rogers, M. T. *J. Magn. Reson.* **1973**, *9*, 92−107.
(59) Schonland, D. S. *Proc. Phys. Soc., London* **1959**, *73*, 788−792.

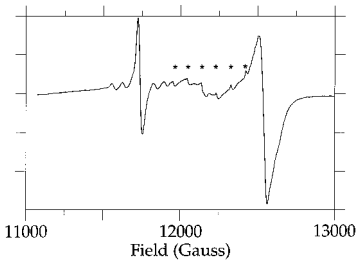

Figure 6. Representative oriented single crystal EPR spectrum of $(Bu_4N)_2[SnBr_6\{MoOBr_5\}]$ along one of the orthogonal crystallographic axes at Q-band (34.117 GHz). Features marked with an asterisk arise from a Mn^{2+} contaminant in the cavity.

The resulting anisotropic EPR parameters for (H$_2$dafone)-[Nb{Mo}OCl$_4$(H$_2$O)]Cl and $(Bu_4N)_2[SnBr_6\{MoOBr_5\}]$ are listed in Table 3 along with the values for the fluoride complex obtained from the literature. While the $g_{\|}$ and $A_{\|}^{Mo}$ values exhibit the same trends as the isotropic parameters, a notable feature of the parameters is the anomalous trend in g values: $g_{\|} > g_{\perp}$ for $[MoOCl_5]^{2-}$ and $g_{\|} > g_e > g_{\perp}$ for $[MoOBr_5]^{2-}$. The values in Table 3 compare well to previously published results on the anions in fluid or frozen solutions[33,39,47a,48,50] or in oriented lattices.[36,39,41,47−49] These values agree well with previous determinations.

Analysis. The aim of our analysis is to provide a relatively straightforward methodology for relating experimental EPR parameters to specific electronic structural features. A simple LCAO model of the relevant electronic states of the complexes is developed below, and generalized expressions for the EPR parameters in terms of electronic parameters are derived. These expressions explicitly incorporate the effects of covalency, halide based spin−orbit coupling, and low-energy charge transfer excited states. Fits of the experimental data to the expressions provide estimates of the electronic structural parameters, which are then used to quantitatively evaluate specific contributions to the EPR parameters. It should be stated clearly at the outset that our aim is *not* to provide reliable values for the bonding coefficients of these complexes. More sophisticated calculational approaches are available for such questions.[60−63] Our aim is to understand the origins of trends in the EPR parameters for a systematically varied series of complexes. As we note further below, the major conclusions of the analysis are relatively insensitive to modest differences in the electronic structural parameters one chooses to employ and the analysis provides considerable insight into the origins of the observed trends.

Molecular Orbital Model. As noted in the Introduction, crystal field treatments of g values do not give meaningful results for many Mo(V) enzyme active sites and model complexes. In particular, such a model is unable to account for the observed ordering of g values for $[MoOCl_4(H_2O)]^-$ and $[MoOBr_5]^{2-}$ or for the unusually large $g_{\|}$ value for $[MoOBr_5]^{2-}$. Since the unpaired electron is considerably delocalized onto the ligand atoms, a molecular orbital treatment is more appropriate for describing the electronic structure. Such treatments, including equations for the calculation of EPR parameters, have been developed previously.[29,37,39,42,47c,64] We present here a modification of the previous treatments which specifically incorporates both charge transfer state contributions and the metal−ligand overlaps. While the essential features of this model are not fundamentally different from those previously developed, they have been chosen to permit a straightforward analysis of the results in terms of specific electronic structural contributions to the EPR parameters.

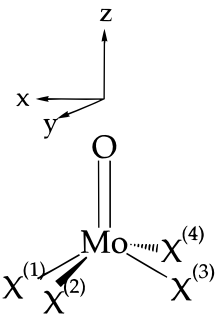

Figure 7. Coordinate system for analysis of C_{4v} $[MoX_4]^-$ complexes. The coordinate systems of each atom are parallel to the indicated molecular system.

A convenient coordinate system for the analysis of the Mo(V) complexes is given in Figure 7. Although in each complex there is a ligand *trans* to the oxo group, we have not explicitly included it. Previous studies[56] of $[Mo^{V}OCl_4(L)]^{n-}$ complexes have shown that the EPR parameters are rather sensitive to the presence or absence of a sixth ligand, but not to its identity. In the model we develop below, any effects from this sixth ligand are subsumed into the oxo group parameters. In this coordinate system, the **g** and $\mathbf{A}^{Mo}$ interaction matrices are diagonal and the following direct correspondences hold: $g_z = g_{\|}$, $g_{x,y} = g_{\perp}$; $A_z = A_{\|}^{Mo}$, $A_{x,y} = A_{\perp}^{Mo}$. Due to the strict axial symmetry of the site, the **g** and $\mathbf{A}^{Mo}$ interaction matrices are required to have collinear principal axes. The point group symmetry of the complexes is C_{4v}, and in the ground state the unpaired electron is located in an orbital which is primarily molybdenum 4d$_{xy}$ in character,[51,52] which is denoted as $|^2B_2\rangle$. Only excited states of b_1 or e symmetry can mix with the ground state under spin−orbit coupling, so that only excited state molecular orbitals transforming as b_1 or e need to be considered. The relevant LCAO wave functions representing the ground and first few excited state MO's are given below:

$$|B_2\rangle = \beta_2|d_{xy}\rangle - \beta_2'|\Phi_{b_2}\rangle \qquad \text{(ground state)}$$

$$|B_1\rangle = \beta_1|d_{x^2-y^2}\rangle - \beta_1'|\Phi_{b_1}\rangle \qquad \text{(ligand field state)}$$

$$|E_x\rangle = \epsilon|d_{xz}\rangle - \epsilon'|\Phi_{e_x}\rangle - \epsilon''|O_{p_x}\rangle \qquad \text{(ligand field state)}$$

$$|E_y\rangle = \epsilon|d_{yz}\rangle - \epsilon'|\Phi_{e_y}\rangle - \epsilon''|O_{p_y}\rangle \qquad \text{(ligand field state)}$$

$$|B_1(CT)\rangle = \chi'|\Phi_{b_1}\rangle + \chi|d_{x^2-y^2}\rangle \qquad \text{(charge transfer state)}$$

The d orbitals are metal-localized and the Φ's represent the appropriate symmetry adapted linear combinations of ligand p orbitals, as given below:

$$|\Phi_{b_2}\rangle = {}^1/_2(p_y^{(1)} + p_x^{(2)} - p_y^{(3)} - p_x^{(4)})$$

$$|\Phi_{b_1}\rangle = {}^1/_2(-p_x^{(1)} + p_y^{(2)} + p_x^{(3)} - p_y^{(4)})$$

$$|\Phi_{e_x}\rangle = {}^1/_{\sqrt{2}}(p_z^{(1)} - p_z^{(3)})$$

$$|\Phi_{e_y}\rangle = {}^1/_{\sqrt{2}}(p_z^{(2)} - p_z^{(4)})$$

Although there are ligand based s valence orbitals of appropriate symmetry to participate in bonding, they have not been explicitly included since the energy separation between the valence s and

(60) Weber, J.; Garner, C. D. *Inorg. Chem.* **1980**, *19*, 2206−2209.
(61) Sunil, K. K.; Harrison, J. F.; Rogers, M. T. *J. Chem. Phys.* **1982**, *76*, 3087−3097.
(62) Deeth, R. J. *J. Chem. Soc., Dalton Trans.* **1991**, 1895−1900.
(63) (a) Swann, J. M.A. Thesis, Wesleyan University, May 1996. (b) Swann, J.; Westmoreland, T. D. To be published.
(64) Sunil, K. K.; Harrison, J. F.; Rogers, M. T. *J. Chem. Phys.* **1982**, *76*, 3078−3086.

p orbitals leads to relatively small contributions. Within the approximations of the model, the ligand s orbital contributions have been subsumed into the p orbitals of similar symmetry; i.e., the p functions in $|\Phi_{b_1}\rangle$ should be more realistically regarded as hybrids with predominantly p character.

g and $\mathbf{A^{Mo}}$ Interaction Matrices. Standard perturbation methods have been employed for deriving expressions for the **g** and $\mathbf{A}^{Mo}$ interaction matrices. The elements of the **g** matrix for an $S = 1/2$ system are obtained from the following perturbation expression.[29,65]

$$g_{ij} = g_e - \Lambda_{ij} \qquad i, j = x, y, z$$

where the Λ_{ij} are given by

$$\Lambda_{ij} = \sum_{n\neq 0} \frac{\langle n|\lambda\hat{L}_i|0\rangle\langle 0|\hat{L}_j|n\rangle + \langle 0|\lambda\hat{L}_i|n\rangle\langle n|\hat{L}_j|0\rangle}{E_n - E_0}$$

In the equations, $|n\rangle$ represents an electronic excited state and $|0\rangle$ is the ground state, $\hat{L}_k$ is the orbital angular momentum operator about the k axis, λ is a spin−orbit coupling constant, and $E_n - E_0$ corresponds to the energy difference between the ground state and excited state $|n\rangle$. The summation is over all of the excited states. The evaluation of the matrix elements over the LCAO wave functions is relatively straightforward and is outlined in the Supporting Information.

The resulting expressions for the principal g values are given below. In the equations, Δg^{LF} and Δg^{CT} correspond to contributions to the g value from ligand field states and the charge transfer state, respectively, λ_i is the one-electron spin−orbit constant for atom i, and S_{b_1}, S_{b_2}, and S_e^i are the overlap integrals between the metal and ligand centered orbitals in the indicated electronic state.

$$g_{\|} = g_e + \Delta g_{\|}^{LF} + \Delta g_{\|}^{CT} \tag{1}$$

$$\Delta g_{\|}^{LF} = \frac{-1}{E_{B_1}}[2\beta_1\beta_2\lambda_{Mo} - (2\beta_1\beta_2'\lambda_{Mo} - \beta_1'\beta_2\lambda_X)S_{b_2} - \beta_1'\beta_2'\lambda_X] \times [2\beta_1\beta_2 - (2\beta_1'\beta_2 - \beta_1\beta_2')S_{b_1} - \beta_1'\beta_2'] + \frac{-1}{E_{B_1}}[2\beta_1\beta_2\lambda_{Mo} - (2\beta_1'\beta_2\lambda_{Mo} - \beta_1\beta_2'\lambda_X)S_{b_1} - \beta_1'\beta_2'\lambda_X] \times [2\beta_1\beta_2 - (2\beta_1\beta_2' - \beta_1'\beta_2)S_{b_2} - \beta_1'\beta_2']$$

$$\Delta g_{\|}^{CT} = \frac{1}{E_{CT}}[2\beta_2\chi\lambda_{Mo} - (2\beta_2'\chi\lambda_{Mo} + \beta_2\chi'\lambda_X)S_{b_2} + \beta_2'\chi'\lambda_X] \times [2\beta_2\chi + (2\beta_2\chi' + \beta_2'\chi)S_{CT} + \beta_2'\chi'] + \frac{1}{E_{CT}}[2\beta_2\chi\lambda_{Mo} + (2\beta_2\chi'\lambda_{Mo} + \beta_2'\chi\lambda_X)S_{CT} + \beta_2'\chi'\lambda_X] \times [2\chi\beta_2 - (2\beta_2'\chi + \beta_2\chi')S_{b_2} + \beta_2'\chi']$$

$$g_{\perp} = g_e + \Delta g_{\perp}^{LF} \tag{2}$$

$$\Delta g_{\perp}^{LF} = \frac{-1}{E_E}[\beta_2\epsilon\lambda_{Mo} - (\beta_2\epsilon'\lambda_{Mo} - (1/\sqrt{2})\beta_2'\epsilon\lambda_X)S_e^X + (1/\sqrt{2})\beta_2'\epsilon'\lambda_X - \beta_2\epsilon''\lambda_{Mo}S_e^O] \times [\beta_2\epsilon - (\beta_2'\epsilon + \beta_2\epsilon')S_{b_2} + (1/\sqrt{2})\beta_2'\epsilon'] + \frac{-1}{E_E}[\beta_2\epsilon\,\lambda_{Mo} - (\beta_2'\epsilon\lambda_{Mo} + \beta_2\epsilon'\lambda_X)S_{b_2} + (1/\sqrt{2})\beta_2'\epsilon'\lambda_X] \times [\beta_2\epsilon - (\beta_2\epsilon' + (1/\sqrt{2})\beta_2'\epsilon)S_e^X - \beta_2\epsilon''S_e^O + (1/\sqrt{2})\beta_2'\epsilon']$$

The hyperfine interaction matrix was obtained by evaluating the Abragam and Pryce Hamiltonian[66] to first order in spin−orbit coupling:

$$A_{ij} = A_{ij}^{(1)} + A_{ij}^{(2)} \qquad i, j = x, y, z$$

$$A_{ij}^{(1)} = A_F - P_M[\xi L(L+1) - {}^3/_2\xi\langle 0|\hat{L}_i\hat{L}_j + \hat{L}_j\hat{L}_i|0\rangle]$$

$$A_{ij}^{(2)} = -P_M[\Lambda_{ij} + 3\xi\Omega_{ij}]$$

where the Λ_{ij} were defined above, and

$$\Omega_{ij} = \frac{-i}{2}\epsilon_{jkl} \times \sum_{n\neq 0}\frac{\langle n|\lambda\hat{L}_l|0\rangle\langle 0|\hat{L}_j\hat{L}_k + \hat{L}_k\hat{L}_i|n\rangle + \langle 0|\lambda\hat{L}_l|n\rangle\langle n|\hat{L}_j\hat{L}_k + \hat{L}_k\hat{L}_i|0\rangle}{E_n - E_0}$$

In these equations, A_F represents the Fermi contact contribution to the hyperfine coupling and $P_M = g_e\beta_e g_N\beta_N\langle r^{-3}\rangle$ evaluated over the ground state wave function. ϵ_{jkl} is the Levi−Civita permutation symbol, and ξ is a numerical factor which takes a value of ${}^2/_{21}$ for a single unpaired d electron. Evaluation of the matrix elements over the LCAO basis gives the expressions for the principal values of the molybdenum hyperfine interaction matrix shown below.

$$A_{\|}^{Mo} = A_F^{Mo} + A_{S\|}^{Mo} + A_{L\|}^{Mo} \tag{3}$$

$$A_{S\|}^{Mo} = -{}^4/_7 P_M\beta_2(\beta_2 - \beta_2' S_{b_2})$$

$$A_{L\|}^{Mo} = \frac{-2P_M}{E_{B_1}}[2\beta_1\beta_2\lambda_{Mo} - (2\beta_1\beta_2'\lambda_{Mo} - \beta_1'\beta_2\lambda_X)S_{b_2} - \beta_1'\beta_2'\lambda_X][\beta_2(\beta_1 - \beta_1' S_{b_1})] - \frac{2P_M}{E_{B_1}}[2\beta_1\beta_2\lambda_{Mo} - (2\beta_1'\beta_2\lambda_{Mo} - \beta_1\beta_2'\lambda_X)S_{b_1} - \beta_1'\beta_2'\lambda_X] \times [\beta_1(\beta_2 - \beta_2' S_{b_2})] - \frac{6}{7}\frac{P_M}{E_E}[\beta_2\epsilon\lambda_{Mo} - (\beta_2'\epsilon\lambda_{Mo} + \beta_2\epsilon'\lambda_X)S_{b_2} + (1/\sqrt{2})\beta_2'\epsilon'\lambda_X] \times [-\beta_2(\epsilon - \epsilon' S_e^X - \epsilon'' S_e^O)]$$

$$A_{\perp}^{Mo} = A_F^{Mo} + A_{S\perp}^{Mo} + A_{L\perp}^{Mo} \tag{4}$$

$$A_{S\perp}^{Mo} = {}^2/_7 P_M\beta_2(\beta_2 - \beta_2' S_{b_2})$$

$$A_{L\perp}^{Mo} = \frac{-P_M}{E_E}[\beta_2\epsilon\lambda_{Mo} - (\beta_2'\epsilon\lambda_{Mo} + \beta_2\epsilon'\lambda_X)S_{b_2} + (1/\sqrt{2})\epsilon'\beta_2'\lambda_X][\beta_2(\epsilon - \epsilon' S_e^X - \epsilon'' S_e^O)] + \frac{-P_M}{E_E}[\beta_2\epsilon\lambda_{Mo} + (1/\sqrt{2})\beta_2'\epsilon'\lambda_X - (\beta_2\epsilon'\lambda_{Mo} + (1/\sqrt{2})\beta_2'\epsilon\lambda_X)S_e^X - \beta_2\epsilon''\lambda_{Mo}S_e^O][\epsilon(1 - \beta_2' S_{b_2})] + \frac{3}{7}\frac{P_M}{E_E}[\beta_2\epsilon\lambda_{Mo} - (\beta_2'\epsilon\lambda_{Mo} + \beta_2\epsilon'\lambda_X)S_{b_2} + (1/\sqrt{2})\beta_2'\epsilon'\lambda_X][\beta_2(\epsilon - \epsilon' S_e^X - \epsilon'' S_e^O)]$$

In eqs 3 and 4, the A_S terms are the spin dipolar contributions

(65) Wertz, J. E.; Bolton, J. R. *Electron Spin Resonance*; Chapman and Hall: New York, 1986; p 279.
(66) Abragam, A.; Pryce, M. H. L. *Proc. R. Soc. London* **1951**, *A79*, 135−153.

Table 4. Constant Parameters Used for Simplex Fits

	X = F	X = Cl	X = Br
λ_{L} (cm^{-1})	272[a]	587[a]	2460[b]
excited state energies			
$E(B_1)$ (cm^{-1})	22 000[c]	23 000[d]	21 800[e]
$E(E)$ (cm^{-1})	13 100[c]	13 000[d]	14 290[e,f]
$E(CT)$ (cm^{-1})		28 000[d]	26 530[e,g]
overlap integrals			
S_{b_2}	0.1946	0.2418	0.1863
S_{b_1}	0.1112	0.1782	0.1806
S_e^L	0.1739	0.2161	0.1665
S_e^O	0.3054	0.3054	0.3054
S_{CT}		0.1782	0.1806

[a] From ref 39. [b] From ref 38. [c] From ref 68. [d] From ref 53. [e] From ref 69. [f] By analogy to $[MoOBr_4(H_2O)]^-$ in ref 52. [g] The assignment was made by analogy to the absorption spectrum of the chloro complex.[45,53]

to the hyperfine interaction. These terms represent the spin−spin dipolar coupling of the nuclear spin with the electronic spin, an effect which is completely anisotropic. The A_L terms are the orbital dipolar contributions and represent the coupling of the electronic orbital angular momentum to the nuclear spin. This contribution has both isotropic and anisotropic components. The Fermi contact contribution, A_F, is completely isotropic.

A number of additional approximations have been used in obtaining eqs 1−4. The O−Mo−X angle was not explicitly taken into account in the calculation of the angular momentum matrix elements. The only anion which has been crystallographically characterized[49b] is $[MoOCl_4(H_2O)]^-$ in which the O−Mo−X angle is 99°, which corresponds to only about 15% $X(p_z)$ character in the ground state $|\Phi_{b_2}\rangle$ orbital. The effects of the O−Mo−X angles *were* taken into account in the estimation of overlap integrals where they are expected to be more important. Also, no contributions from charge transfer excited states were included in the expressions for $g_\perp$, $A_\parallel^{Mo}$, or $A_\perp^{Mo}$. The observed $\Delta g_\perp$ shifts are small and reliable assignments of the ^2E charge transfer excited states are not available for all of the species. Any charge transfer effects on $g_\perp$ are therefore subsumed into the ^2E ligand field state parameters. Likewise, excited state contributions to $A_\parallel^{Mo}$ are small, and any charge transfer contributions are incorporated into the overall $^2B_1$ or ^2E parameters. The use of these approximations has no significant effects on the ultimate conclusions from this analysis and afford a considerable degree of calculational and interpretive simplicity. It should also be noted that calculation of EPR parameters for these species directly from the output of density functional routines yield similar parameters and identical conclusions.[63] Thus eqs 1−4 represent a relatively complete treatment of the EPR parameters of an axially symmetric d^1 system and retains much of the interpretive transparency of the LCAO approach.

A nonlinear simplex fitting procedure[67] was used to find the best set of LCAO coefficients which simultaneously reproduces the experimental g and A^{Mo} values for each ion. Values for λ_X, and the excited state energies were taken from the literature and are summarized in Table 4. The overlap integrals were estimated on the basis of direct evaluation of the overlap of two appropriately defined Slater-type orbitals.[70] In the simplex fitting routines the values of the molecular orbital coefficients, A_F, and λ_{Mo}, were allowed to vary. Values for P_M were obtained from the relationship $P_{Mo} = -15.895\lambda_{Mo}$.[37] The function minimized was

$$F = \frac{(g_\parallel(\text{obs}) - g_\parallel(\text{calc}))^2}{g_\parallel(\text{obs})^2} + \frac{(g_\perp(\text{obs}) - g_\perp(\text{calc}))^2}{g_\perp(\text{obs})^2} + \frac{(A_\parallel^{Mo}(\text{obs}) - A_\parallel^{Mo}(\text{calc}))^2}{(A_\parallel^{Mo}(\text{obs}))^2} + \frac{(A_\perp^{Mo}(\text{obs}) - A_\perp^{Mo}(\text{calc}))^2}{(A_\perp^{Mo}(\text{obs}))^2}$$

Table 5. Simplex Optimized Electronic Structural Parameters

	X = F	X = Cl	X = Br
β_2	1.008	0.9590	0.9297
β_1	0.6966	0.8245	0.8162
ϵ	0.9559	0.8973	0.8223
ϵ'	0.0686	0.1636	0.2682
χ		0.2444	0.2292
A_F (10^{-4} cm^{-1})	53.98	42.78	39.92
λ_M (cm^{-1})	911.4	933.8	901.6
P_M (cm^{-1})	−57.34	−58.75	−56.72

The simplex fitting procedure found only one minimum for each complex, and the best fit parameters obtained for each complex are given in Table 5. Systematic exploration of physically meaningful parameter space showed no other significant minima. The values in the table fit the experimentally observed EPR parameters exactly within the experimental precision limits. Statistical analysis of the variances of these values was not possible due to the small number of observables. By independently varying each fit parameter to determine the point at which the difference between the calculated and observed EPR parameters would exceed the resolution of the experimental data, the precision of the parameters was estimated to be ±2%. However, the fits require several input parameters from other experiments (e.g., excited state energies and ligand spin−orbit coupling constants) or that must be estimated by a separate calculation (i.e., the overlap integrals). The best fit LCAO coefficients are sensitive (±5%) to modest variations in these parameters, and it is clear that the exact magnitudes of the "best fit" parameters in Table 5 provide only an approximation to the "true" wave functions. In the analysis of the EPR parameters presented below, however, these variations tend to cancel and the interpretation of the results is not particularly sensitive to the choice of fixed parameters for the fits.

Discussion

Electronic Structure. The parameters in Table 5 provide a means of estimating Mulliken populations and atomic orbital contributions to the estimated molecular wave functions. Table 6 summarizes the population analysis on the basis of the results of the simplex fits. The electronic structures of the ground states and the relevant excited states agree qualitatively with expectations from general bonding principles and compare reasonably well with the few calculations available on these systems.[60−63]

(67) Algorithm AS 47: O'Neill, R. *Appl. Stat. (J. R. Stat. Soc. C)* **1971**, *20*, 338−345.
(68) Wentworth, R. A. D.; Piper, T. S. *J. Chem. Phys.* **1964**, *41*, 3884−3889.
(69) Allen, E. A.; Brisdon, B. J.; Edwards, D. A.; Fowles, G. W. A.; Williams, R. G. *J. Chem. Soc.* **1963**, 4649−4657.
(70) Westmoreland, T. D. Unpublished results. The orbitals were of the general form $Nx^a y^b z^c r^{(n*-d)} \exp(-Z*r/n*)$ where $a + b + c = l$, $d = l + 1$, and $Z*$ and $n*$ are the effective values of nuclear charge and principal quantum number taken from either the Clementi−Raimondi rules or Slater's rules. The overlaps were calculated by direct numerical integration of the product of two such functions centered at a distance R_{Mo-L} from each other. The program gave values which agreed with previously published tabulations of overlap integrals between Slater functions.[71] The overlap integrals were adjusted by the appropriate angular overlap factors[72] for the O−Mo−X angles (99° for X = Cl[49b] and estimated as 105° for X = F and Br[61]).
(71) Mulliken, R. S.; Rieke, C. A.; Orloff, D.; Orloff, H. *J. Chem. Phys.* **1949**, *17*, 1248−1267.
(72) Larsen, E.; La Mar, G. N. *J. Chem. Educ.* **1974**, *51*, 633−640.

Table 6. Mulliken Population Analysis[a]

state		X = F	X = Cl	X = Br
B_2	M	0.9482	0.7809	0.7639
	X	0.0518 (0.0129)	0.2191 (0.0548)	0.2361 (0.0590)
B_1	M	0.4234	0.5722	0.5566
	X	0.5766 (0.1441)	0.4278 (0.1070)	0.4434 (0.1108)
E	M	0.6900	0.5465	0.4199
	X	−0.0067 (−0.0017)	−0.0050 (−0.0013)	0.0352 (0.0088)
	O	0.3167	0.4584	0.5449
CT	M		0.1001	0.0912
	X		0.8999 (0.2250)	0.9088 (0.2272)

[a] Values in parentheses represent the values per atom.

Table 7. Specific Electronic Contributions to Net g Values

	X = F	X = Cl	X = Br
$g_{\|\|}$	1.894	1.9632	2.090
no covalency	1.839	1.8140	1.824
no ligand spin−orbit	1.889	1.9282	1.932
no charge transfer		1.9070	1.969
$g_\perp$	1.913	1.9400	1.945
no covalency	1.873	1.8960	1.929
no ligand spin−orbit	1.913	1.9404	1.958

The ground state of the fluoride complex is the least covalent, as expected, with ∼95% metal character. The chloride and bromide complexes show very similar metal characters, ∼76−78%, and thus very similar ground state covalencies. The similarity in the metal characters of the ground states of the chloride and bromide complexes is due to the effects of the overlap population. The B_1 excited states are all significantly more covalent than the ground state, a result which is consistent with the role of the $d_{x^2-y^2}$ orbital in σ bonding to the halide ligands. For each complex, the E excited state contains very little contribution from the equatorial ligands and is dominated by the Mo−O π interaction. Down the halide series, this orbital becomes more oxygen-localized, as expected on the basis of the increasing ease of oxidation of the metal. For the chloride and bromide complexes the parameters for the B_1 LMCT excited state suggest nearly complete transfer of charge.

Origin of *g* Values. The parameters in Table 5 provide a means of analyzing specific contributions to the observed EPR parameters in these systems. In particular, it is important to understand how covalency, ligand spin−orbit coupling, and charge transfer states *quantitatively* manifest themselves in the EPR parameters. The results of such an analysis are given in Table 7. In the table, "no covalency" refers to a calculation of the g values from eqs 1 and 2 using the parameters of Table 5, but with all ligand coefficients, metal−ligand overlap integrals, and ligand spin−orbit coupling constants set to zero. This limit corresponds approximately to a crystal field treatment. In each case, the calculated g value is significantly smaller than the observed value. This result confirms that the ligand-based terms in eqs 1 and 2 yield a net positive contribution to the g value, in contrast to the purely metal-based terms. The quantitative magnitude of the covalency contribution to $g_{\|}$ increases in the order F < Cl < Br. Since the ground state metal characters of the chloride and bromide complexes are similar, it is interesting that the calculated g values in the absence of covalency are so different. It is clear that the covalencies of both the B_1 ligand field excited state and the B_2 ground state are of equal importance in determining the value of $g_{\|}$. For $g_\perp$, in contrast, the covalency contributions are much less variable across the series, an effect which is due to the dominance of the Mo−O interaction in the relevant E excited state.

The preceding analysis provides some insight into the electronic structural requirements for obtaining $g_{\|} > g_\perp$, a result which cannot be realized from the crystal field model. For both the chloride and the bromide complexes, ignoring covalency switches the order of the calculated g values to $g_\perp > g_{\|}$. Also, in the absence of metal−ligand covalency $g_{\|}$ is predicted to be smaller than g_e for the bromide complex. Thus, the covalencies of the ground and B_1 excited states play the dominant roles in causing the g value reversal common in these and related systems and are also important for producing g values greater than g_e.

Table 8. Components of Net A^{Mo} Values[a]

	X = F	X = Cl	X = Br
A_F	53.98	42.78	39.92
$A_{L,\|\|}$	5.05	5.70	1.32
$A_{L,\perp}$	4.06	2.92	2.46
$A_{S,\|\|}$	31.07	26.21	24.76
$A_{S,\perp}$	−15.53	−13.11	−12.38

[a] All values are in units of 10^{-4} cm^{-1}.

The entries in Table 7 corresponding to "no ligand spin−orbit" refer to the calculated g values using the values in Table 5 but with $\lambda_L = 0$. Removing the ligand spin−orbit coupling also tends to lower the g values, but in each case the effect is significantly smaller than that of eliminating metal−ligand covalency. The effects of ligand spin−orbit coupling clearly become more important as the ligand spin−orbit constant increases, but even with a very large constant, the contribution is still smaller than that due to covalency. Ligand spin−orbit coupling contributes less to $g_\perp$ values, but for the chloride and bromide complexes the relative ordering of the calculated g values becomes $g_\perp > g_{\|}$ in the absence of ligand spin−orbit coupling. Thus, significant ligand spin−orbit coupling can lead to the inverted ordering of g values.

For the chloride and bromide complexes, the elimination of the LMCT excited state term , $\Delta g_{\|}^{CT}$, in eq 1 leads to the "no charge transfer" entries in Table 7. In each case elimination of the contribution lowers the value of $g_{\|}$ somewhat and for the chloride complex lowers $g_{\|}$ enough to lead to $g_{\|} < g_\perp$. In the bromide complex, however, on elimination of the charge transfer term the inverted g value ordering is retained, but $g_{\|}$ is lowered enough that $g_e > g_{\|}$.

For the complexes under investigation, the results in Table 7 indicate that metal−ligand covalency, ligand spin−orbit coupling, and low-lying charge transfer (CT) excited states all provide significant contributions to the observed g values. The covalencies of the ground state and relevant excited states provide the dominant contributions, while ligand spin−orbit coupling and charge transfer states provide somewhat smaller effects. Thus, in order to observe $g_{\|} > g_\perp$ the covalency of the ground and B_1 excited states must be quite large, or moderate covalency in addition to low-lying charge transfer excited states of the proper symmetry or large ligand spin−orbit coupling constants are required. In order to obtain g values greater than g_e, large covalencies, low-lying CT excited states, and significant ligand spin−orbit coupling are required. Even in this case, however, the large metal−ligand covalencies are the most important single contribution.

Molybdenum Hyperfine Coupling Constants. In Table 8, the observed molybdenum hyperfine coupling constants have been partitioned into Fermi contact, spin dipolar, and orbital dipolar contributions via eqs 3 and 4 and the parameters in Table 5. In each complex, the isotropic Fermi contact term has the largest magnitude, followed by the spin dipolar contributions. The orbital dipolar terms represent the smallest contributions to the observed hyperfine coupling constants. The small value of the orbital dipolar terms is not surprising. All of the g values

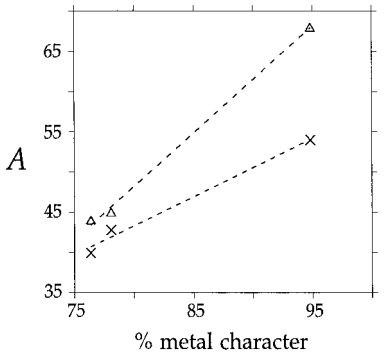

Figure 8. Plots of A_{iso}^{Mo} (Δ) and A_F (×) as a function of ground state metal character.

of the complexes are close to g_e. Since the deviations from $g = g_e$ arise from orbital angular momentum, it is expected that small values of Δg would be associated with only small orbital contributions to the hyperfine interaction. The small orbital angular momenta for these systems can be rationalized in terms of the large ligand field splittings of the second row transition metals, resulting larger energy denominators in the spin−orbit perturbation terms. In fact, inspection of the A_L values show that they parallel the changes in g across the series. The spin dipolar (A_S) contributions primarily reflect changes in the ground state covalency and therefore parallel the values of β_2 for each complex. Since the majority of the anisotropy in A^{Mo} arises from the spin dipolar contribution, it may be expected that the hyperfine anisotropy increases with increasing metal character in the ground state. This is indeed evident from the data in Table 3.

The Fermi contact term arises from direct mixing of molybdenum s orbital character into the ground state wave function and indirectly from spin polarization of core s electrons.[73] Thus, A_F might be expected to be approximately proportional to the ground state metal character. Since the A_{iso}^{Mo} value contains only contributions from A_F and A_L, and since A_L is less than 10% of A_F, it might also be predicted that A_{iso}^{Mo} would correlate with the ground state metal character. For the three complexes analyzed here, this seems to be the case. Figure 8 shows that both A_F and A_{iso}^{Mo} give the predicted trend. Thus, for this series of complexes the experimentally determined average molybdenum hyperfine coupling or the molybdenum hyperfine anisotropy can give a direct estimate of the ground state wave function. Whether such simple correlations are applicable to complexes of lower symmetry is currently under investigation.[74]

An analysis of the molybdenum hyperfine coupling constants similar to that given in Table 7 is included in the Supporting Information. The analysis indicates that the A^{Mo} values are not particularly sensitive to metal−ligand covalency or to ligand spin−orbit coupling. This result is not surprising since, on the basis of eqs 3 and 4, these contributions will primarily affect A_L terms. Since these terms represent only a small fraction of the net hyperfine coupling, no strong dependence on ligand-based terms is expected.

Implications for Other Mo(V) Sites. As noted in the Introduction, much Mo(V) chemistry in recent years has been stimulated by the relevance to the active sites of molybdenum oxidoreductases. The analysis given above suggests an approach to the quantitative interpretation of the observed EPR parameters in these systems in terms of fundamental electronic structural features. The analysis summarized in Table 7 implies that ligand spin−orbit coupling exerts only modest effects on the observed g values. For those model compounds in Table 2 with at least one g value greater than g_e, only $[MoO(SePh)_4]^-$ and Tp^*MoOBr_2 have ligands with very large spin−orbit coupling constants. There is currently no evidence for an atom with such a high spin−orbit coupling constant in the immediate coordination sphere of molybdenum in any of the enzyme active site derivatives.[75] For the active sites of the enzymes in Table 1, the largest reasonable spin−orbit constant would be that of sulfur ($\lambda \approx -320$ cm^{-1}),[76] which is not large enough to directly contribute significantly to the anomalously high g values. Thus ligand spin−orbit coupling may be ruled out as a principal determinant of the EPR parameters of oxidoreductase active sites.

Metal−ligand covalency, in contrast, is probably the most important single electronic structural contributor to the g values. On the basis of the preceding analysis, as the site becomes more covalent in the plane perpendicular to the strongest ligand field, the contributions to the perturbation expressions from ligand-based terms increase and the g values are predicted to approach g_e. These predictions are confirmed in the parameters for the model complexes in Table 2. For example, by comparing *cis*-MoO(OH)L to *cis*-MoO(SH)L it is apparent that replacing hydroxide by hydrosulfide results in an increase in all g values. The corresponding decrease in A_{iso}^{Mo} is also consistent with a more covalent site. Similar comparisons can be made between $Tp^*MoO(OPh)_2$ and $Tp^*MoO(SPh)_2$ and in the series Tp^*MoOX_2 (X = F, Cl, Br). Such effects are only evident when the covalency is increased in the plane of the orbital containing the unpaired electron. For example, Tp^*MoSCl_2 has lower g values than Tp^*MoOCl_2.[36]

To a significant extent, the nearly isotropic parameters for most of the enzyme active sites must arise primarily from the significant metal−ligand covalency. The proposed structures of the various EPR active enzyme active site derivatives[6,22] are consistent with both the g value analysis and the expectations from the molybdenum hyperfine analysis. The most covalent site is predicted to be xanthine oxidase very rapid, a proposed $\{MoOS\}^+$ site. Very rapid is also the xanthine oxidase derivative with the smallest $\langle A^{Mo} \rangle$. By applying the correlation of A_{iso}^{Mo} with ground state metal character given in Figure 8, the ground state covalencies of the xanthine oxidase sites can be estimated: very rapid, 64% Mo; rapid type 1, 72% Mo; rapid type 2, 71% Mo; slow, 74% Mo. For low-pH sulfite oxidase, the ground state covalency is similarly estimated to be 68%. No other average molybdenum hyperfine values for enzyme active sites are currently available.

For several of the active site derivatives in Table 1, the highest g value is greater than g_e. The analysis given above implies that for such a case, both significant metal−ligand covalency and significant contributions from low-lying charge transfer excited states must be involved. For the oxidoreductase sites, the most reasonable excited state would correspond to dithiolene to molybdenum charge transfer. There is evidence for such low-lying charge transfer states in molybdenum thiolate model complexes (e.g., Tp^*MoO(1,2-ethanedithiolate) and Tp^*MoO(toluene-3,4-dithiolate))[53] and from the Mo sites in two bacterial DMSO reductases.[77,78] The implication is that in, for example,

(73) Abragam, A.; Bleaney, B. *Electron Paramagnetic Resonance of Transiton Ions*; Dover: New York, 1986; pp 680−712.
(74) Nipales, N. S.; Westmoreland, T. D. Work in progress.
(75) Halide binding to sulfite oxidase has been shown to be coupled to the high-pH−low-pH transition, however, and may in part account for the large observed increase in the g value[18]).
(76) Estimated from the splitting of the ^{2}P state of $S^-(g)$: Lineberger, W. C.; Woodward, B. W. *Phys. Rev. Lett.* **1970**, *25*, 424−427.
(77) Benson, N.; Farrar, J. A.; McEwan, A. G.; Thomson, A. J. *FEBS Lett.* **1992**, *307*, 169−172.
(78) Finnegan, M. G.; Hilton, J.; Rajagopalan, K. V.; Johnson, M. K. *Inorg. Chem.* **1993**, *32*, 2616−2617.

the xanthine oxidase very rapid site, the orbital which contains the unpaired electron is oriented such that it has a significant charge transfer interaction with the dithiolene of the cofactor, but in the other EPR active derivatives it does not. Clearly, as the coordination environment, and thus the ligand field, of the molybdenum changes, the orientation of the orbital with the unpaired electron will change to remain perpendicular to the direction of strongest ligand field. These considerations suggest a basis for describing how the redox active orbital changes orientation along the overall reaction coordinate.

While these results are suggestive, clearly more detailed work is necessary to understand the electronic structures of these sites. In particular, the detailed analysis of complexes of lower symmetry with more directly relevant ligating atoms (i.e., sulfur) is required. Of additional interest are the quantitative origins of ligand hyperfine splittings. The oxyhalide complexes are particularly difficult to analyze in this respect because of the large number of overlapping hyperfine features. Related complexes with only two halides are currently under investigation.[34,74]

Acknowledgment. The authors gratefully acknowledge the assistance of Dr. R. Weber of Bruker Instruments in obtaining Q-band EPR data, Mr. D. Albert of Wesleyan University for the design of the concentrated acid EPR cell, Prof. P. K. Ross for helpful discussions, and Prof. A. A. Gewirth and Prof. E. I. Solomon for preprints of work prior to publication. The donors of the Petroleum Research Fund, administered through the American Chemical Society, and the National Institutes of Health are also acknowledged for support.

Supporting Information Available: Text describing data collection and structure solution and refinement, figures showing ORTEP diagrams and a unit cell view, and tables giving crystal data and structure refinement, atomic coordinates and isotropic diaplacement parameters, bond distances and angles, anisotropic displacement parameters, torsion angles, and hydrogen coordinates for (H_2dafone)[$NbOCl_4(H_2O)$]Cl, text describing the evaluation of a representative matrix element, and a table of specific electronic structural contributions to the molybdenum hyperfine coupling constants (16 pages). Ordering information is given on any current masthead page.

IC951142A